Supporting Information

Unprecedented Enhancement of Ca^{2+} affinity using a redox-switchable coordinating group

Juan Pedro Merino,[a,b] Adrián M. Abelairas,[a] Javier Hernández-Ferrer,[c] Ana M. Benito,[c] Wolfgang K. Maser,[c] José L. Vilas-Vilela,[b,d] David Esteban-Gómez,[a] Alejandro Criado,[a] Jesús Mosquera,*[a] Carlos Platas-Iglesias,*[a]

[a]Universidade da Coruña, CICA – Centro Interdisciplinar de Química e Bioloxía, Rúa as Carballeiras, 15071 A Coruña, Spain.

[b] Macromolecular Chemistry Research Group (labquimac), Department of Physical Chemistry, Faculty of Science and Technology, University of the Basque Country (UPV/EHU), 48940 Leioa, Spain.

[c] Instituto de Carboquímica (ICB-CSIC) C/ Miguel Luesma Castán 4, 50018 Zaragoza, Spain.

[d] BC Materials, Basque Center for Materials, Applications and Nanostructures, UPV/EHU Science Park, 48940 Leioa, Spain.

Table of Contents

1. Materials and Chemicals

The materials used in this work for synthesis were purchased from BLD pharm and Merck and used as received.

Proton nuclear magnetic resonance (^{1}H NMR) and carbon nuclear magnetic resonance (^{13}C NMR) spectra were obtained on Bruker AVANCE III HD 400 Nuclear Magnetic Resonance spectrometer and were referenced relating to residual proton resonances in $CDCl_3$ (at d 7.26 ppm and 77.23 ppm).

The electrochemical behaviors of the different species were evaluated using cyclic voltammetry (CV) with an electrochemical workstation Autolab MSTAT204 potentiostat/galvanostat (Metrohm). The measurements were performed in a solution containing 0.1 M tetrabutylammonium hexaflorophosphate (TBAPF) as the supporting electrolyte. A three-electrode conformation with a Glassy Carbon as a working electrode, platinum wire as auxiliary electrode and silver wire as pseudo-reference electrode were used. The sample was degassed with nitrogen gas 10 min prior to the scan. After the measurement, ferrocene was added to the sample solution, and CV measurement was performed to confirm the electrode potential.[1]

2. Synthesis of Compounds

Synthesis of 2-(bromomethyl)-6-nitropyridine (2)

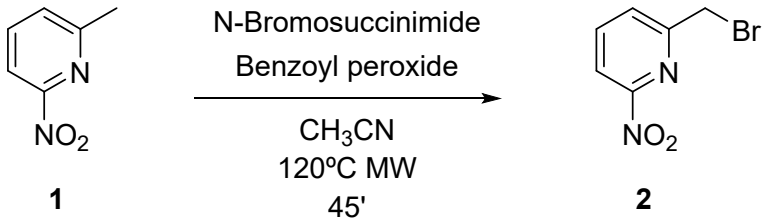

To a solution of 2-methyl-6-nitropyridine (**1**, 395 mg, 2.5 mmol) in MeCN (3 mL) were added N-bromosuccinimide (528 g, 3 mmol) and benzoyl peroxide (60 mg, 0.25 mmol). The reaction mixture was heated at 120 °C under microwave irradiation for 45 min, cooled down to room temperature, and concentrated under reduced pressure. The residue was diluted with 1 M NaOH (5 mL) and extracted with EtOAc (3 × 7.5 mL). The extracts were combined, dried over $MgSO_4$, and concentrated under reduced pressure. The residue was purified by flash column chromatography (silica gel, hexane ramping to AcOEt/hexane = 1:5) to obtain **2** (206.17 mg, 0.95 mmol, 38 %) as a yellow solid.

^{1}H NMR (500 MHz, $CDCl_3$), δ: 8.19 (d, *J* =7.6 Hz, 1H), 8.08 (t, *J* = 7.8 Hz, 1H), 7.88 (d, *J* = 7.6 Hz, 1H), 4.64 (s, 2H) ppm.

^{13}C NMR (125 MHz, $CDCl_3$), δ: 157.35 (2C), 141.01 (CH), 129.17 (CH), 117.19 (CH), 31.61(CH_2) ppm.

HRMS (ESI) for $C_6H_5BrN_2O_2$, $[M+H]^+$, calculated: 216.953, found: 216.961.

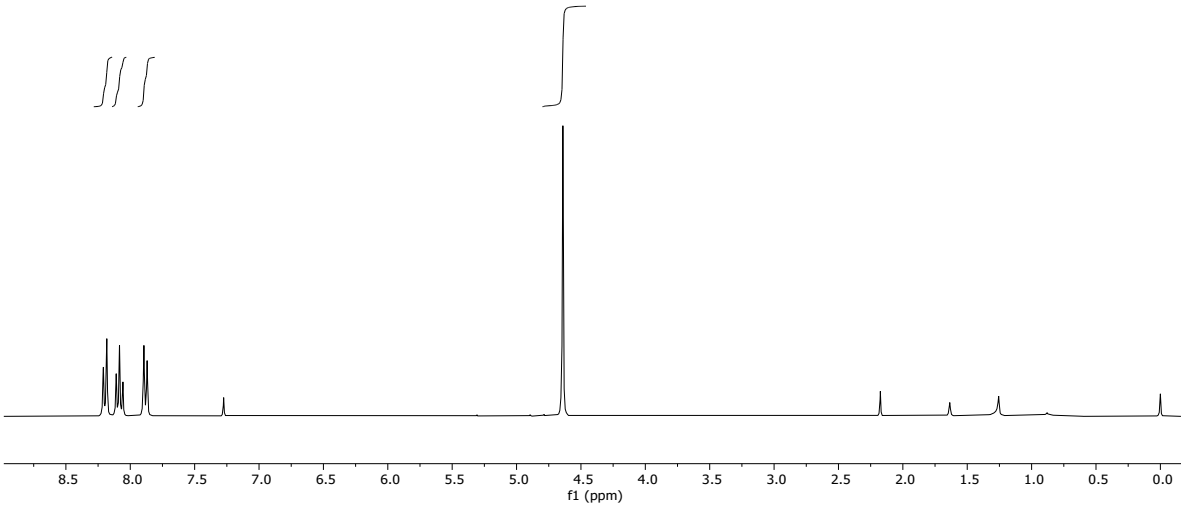

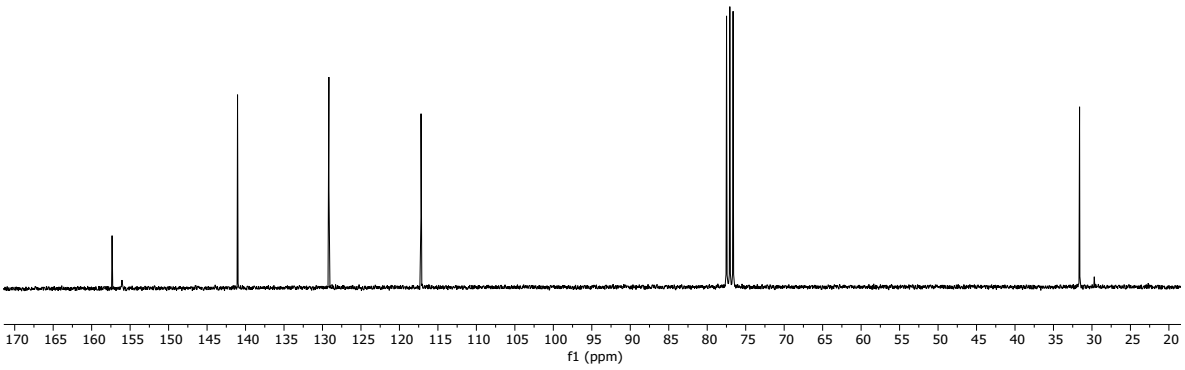

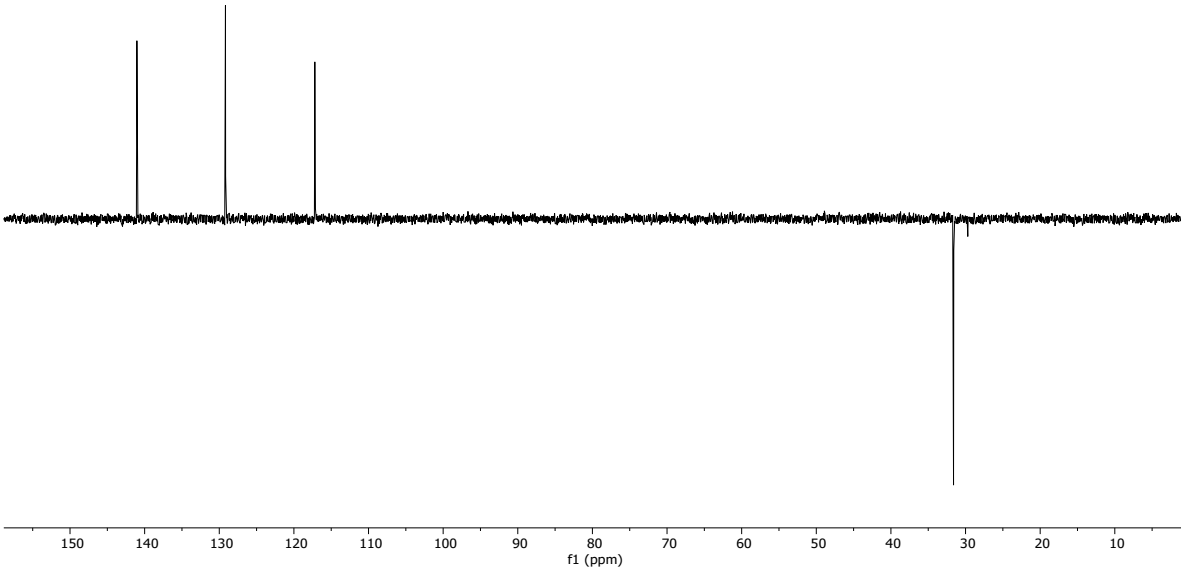

Synthesis of 7,16-bis((6-nitropyridin-2-yl)methyl)-1,4,10,13-tetraoxa-7,16-diazacyclooctadecane (L_1).

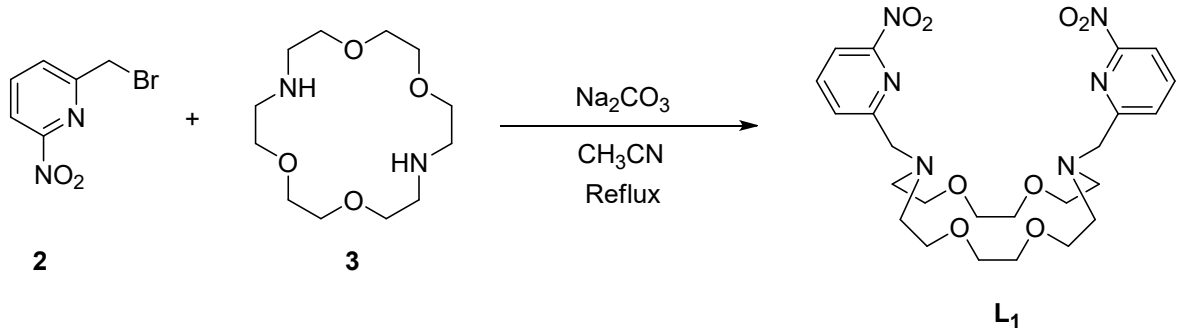

2 **3** **L_1**

A mix of 2-(bromomethyl)-6-nitropyridine (**2**, 104 mg, 0.48 mmol) and Na_2CO_3 (152.5 mg, 1.44 mmol) were added to a solution of 4,13-diaza-18-crown-6 (**3**, 66 mg, 0.25 mmol) in acetonitrile (4.8 mL). The resulting mixture was stirred under reflux for 48 h. It was then filtered, the filtrate was concentrated and the yellow oily residue was extracted with CH_2Cl_2/water. The organic phase was dried with anhydrous $MgSO_4$ and concentrated in a rotary evaporator to give **L_1** (128.3 mg, 0.24 mmol, stoichiometry yield) as a brown oil.

^{1}H NMR (500 MHz, $CDCl_3$), δ: 8.11 (m, 4H), 8.00 (t, J = 7.8 Hz, 2H), 4.00 (s, 4H), 3.64 (t, J = 5.5 Hz, 8H), 3.58 (s, 8H), 2.91 (t, J = 5.5 Hz, 8H) ppm.

^{13}C NMR (125 MHz, $CDCl_3$), δ: 161.98 (2C), 156.13 (2C), 140.02 (2CH), 128.48 (2CH), 115.92 (2CH), 70.75 ($4CH_2$), 69.77 ($4CH_2$), 60.78 ($2CH_2$), 54.67 ($4CH_2$) ppm.

HRMS (ESI) for $C_{24}H_{34}N_6O_8$ $[M+H]^+$, calculated: 535.244, found: 535.251.

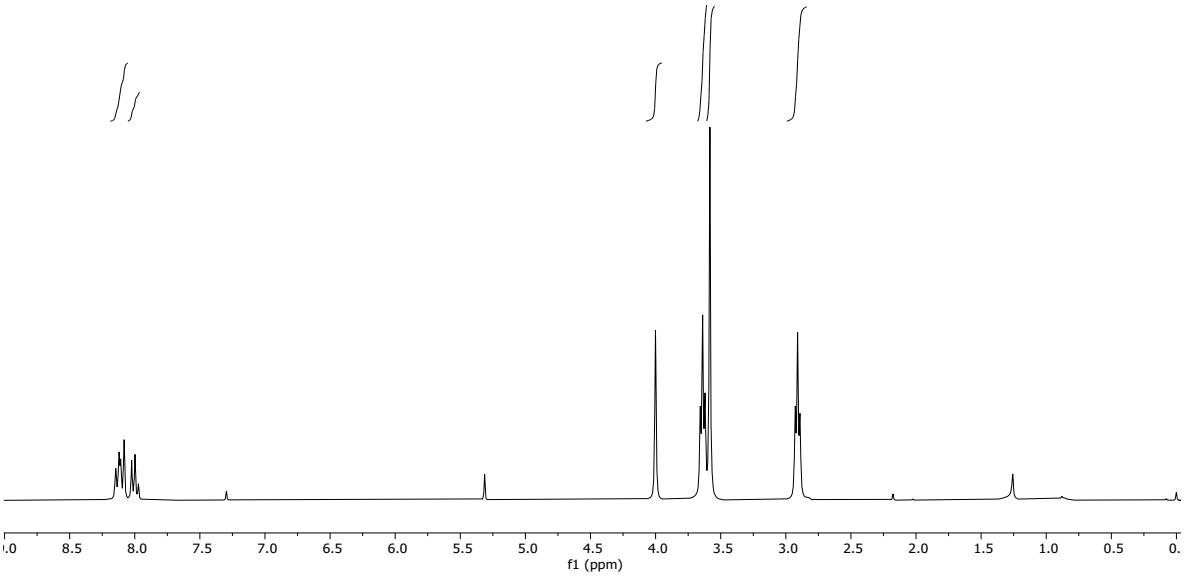
8.5
8.0
7.5
7.0
6.5
6.0
5.5
5.0
4.5
4.0
3.5
3.0
2.5
2.0
1.5
1.0
0.5
f1 (ppm)

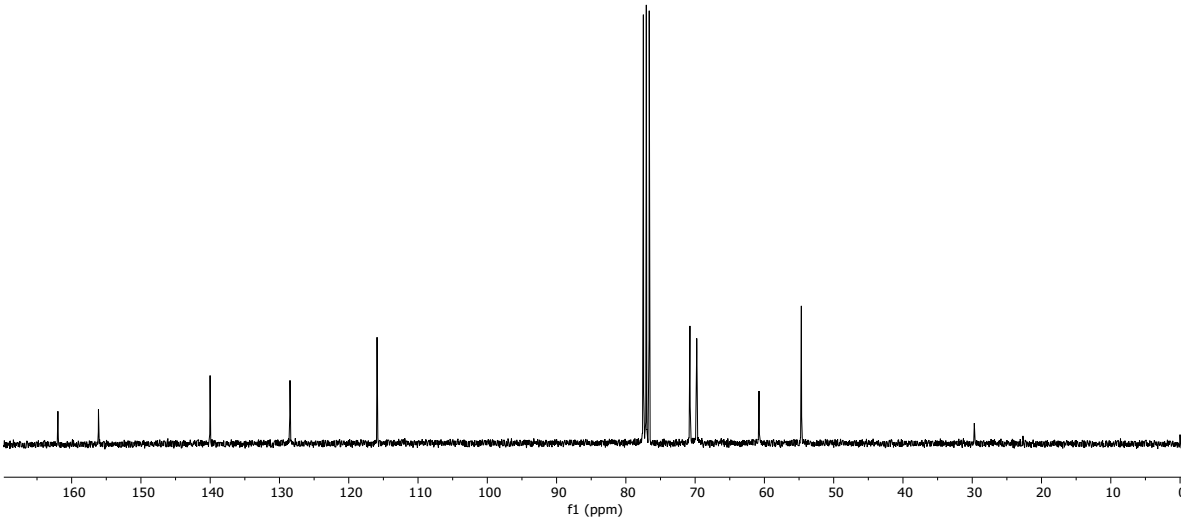
160
150
140
130
120
110
100
90
80
70
60
50
40
30
20
10
f1 (ppm)

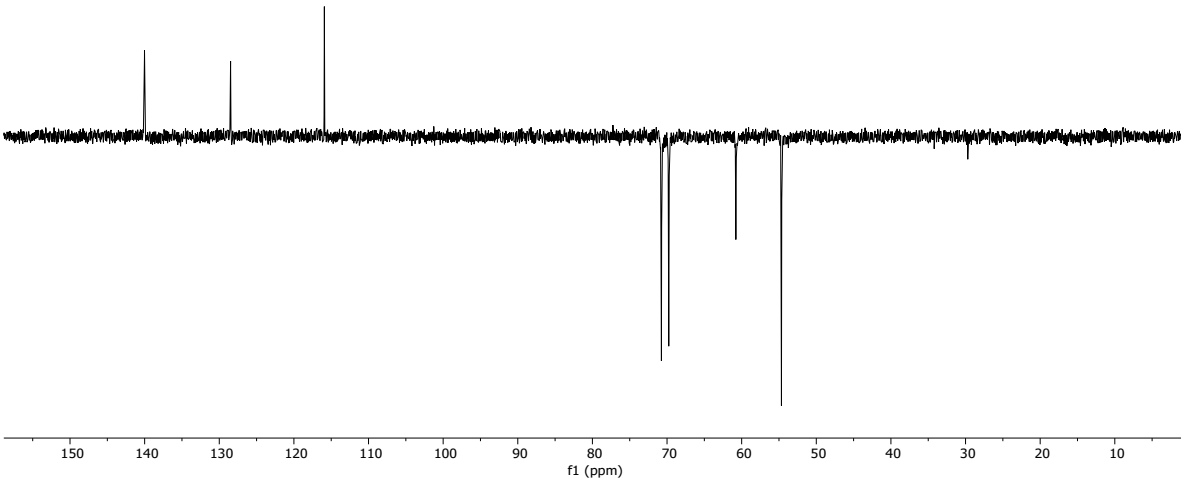

Synthesis of 16-((6-nitropyridin-2-yl)methyl)-1,4,7,10,13-pentaoxa-16-azacyclooctadecane (L_2).

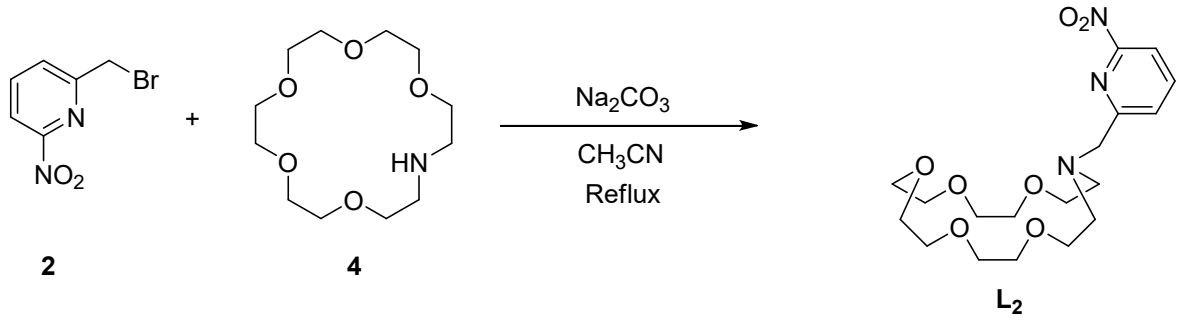

2 **4** **L_2**

A mix of 2-(bromomethyl)-6-nitropyridine (**2**, 30 mg, 0.14 mmol) and Na_2CO_3 (43.9 mg, 0.42 mmol) were added to a solution of 1,4,7,10,13-pentaoxa-16-azacyclooctadecane (**4**, 36 mg, 0.14 mmol) in acetonitrile (1.3 mL). The resulting mixture was stirred under reflux for 48 h. It was then filtered, the filtrate was concentrated and the yellow oily residue was extracted with CH_2Cl_2/water. The organic phase was dried with anhydrous $MgSO_4$ and concentrated in a rotary evaporator to give **L_2** (55.12 mg, 0.14 mmol, stoichiometry yield) as a brown oil.

^{1}H NMR (500 MHz, $CDCl_3$), δ: 8.20 (d, J = 7.5 Hz, 1H), 8.08 (d, J = 7.8 Hz, 1H), 8.01 (s, J = 7.7 Hz, 1H), 4.00 (s, 2H), 3.64 (m, 20H), 2.87 (t, J = 5.4, 4H) ppm.

^{13}C NMR (125 MHz, $CDCl_3$), δ: 160.23 (C), 156.11 (C), 141.10 (CH), 128.93 (CH), 115.80 (CH), 70.65 ($4CH_2$), 70.30 ($4CH_2$), 69.65 (CH_2), 54.67 ($4CH_2$) ppm.

HRMS (ESI) for $C_{24}H_{34}N_6O_8$ $[M+H]^+$, calculated: 400.201, found: 400.207.

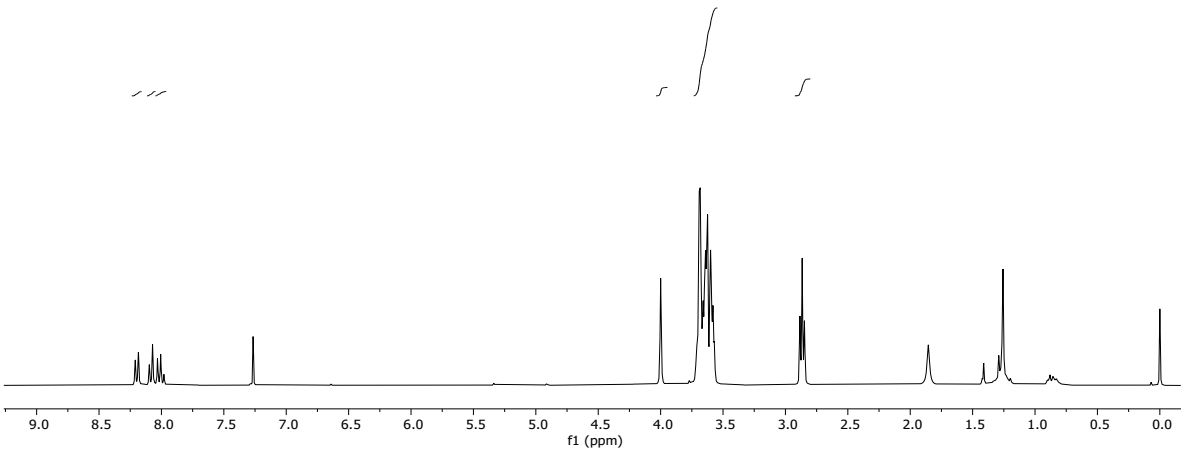
9.0 8.5 8.0 7.5 7.0 6.5 6.0 5.5 5.0 4.5 4.0 3.5 3.0 2.5 2.0 1.5 1.0 0.5 0.0
f1 (ppm)

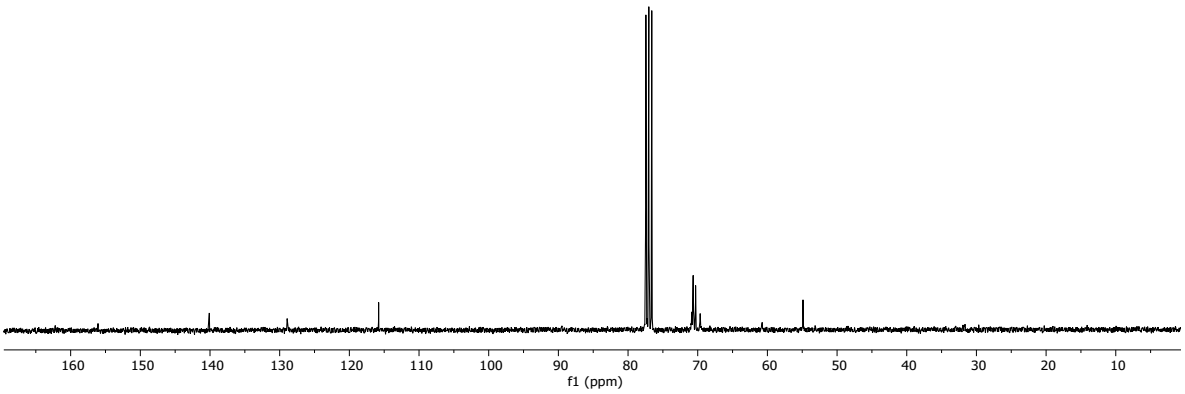
160 150 140 130 120 110 100 90 80 70 60 50 40 30 20 10
f1 (ppm)

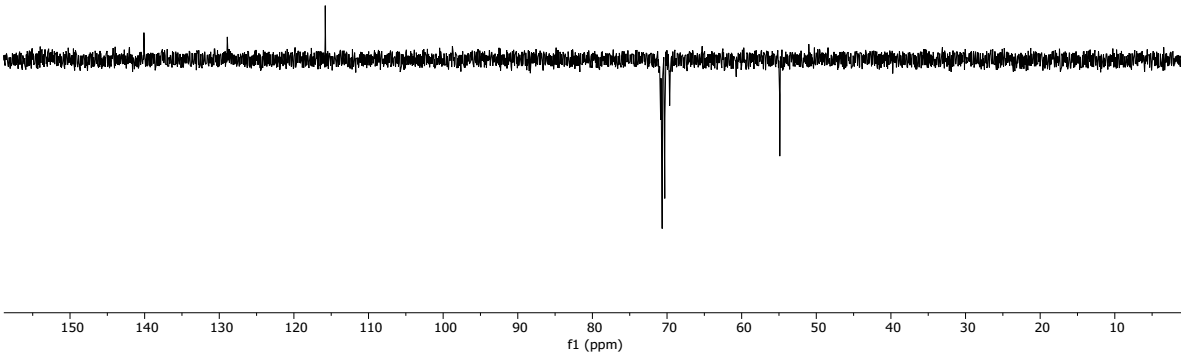
150 140 130 120 110 100 90 80 70 60 50 40 30 20 10
f1 (ppm)

3. Electrochemical Measurements

$$Ar\text{-}NO_2 \underset{E_1}{\overset{+e^-}{\rightleftharpoons}} (Ar\text{-}NO_2)^{\bullet -}$$

$$(Ar\text{-}NO_2)^{\bullet -} \overset{+e^-}{\rightleftharpoons} (Ar\text{-}NO_2)^{2-}$$

$$(Ar\text{-}NO_2)^{\bullet -} + 4H^+ \underset{E_2}{\overset{+3e^-}{\rightleftharpoons}} Ar\text{-}NHOH + H_2O$$

Scheme S1. Reduction of aryl nitro compounds.

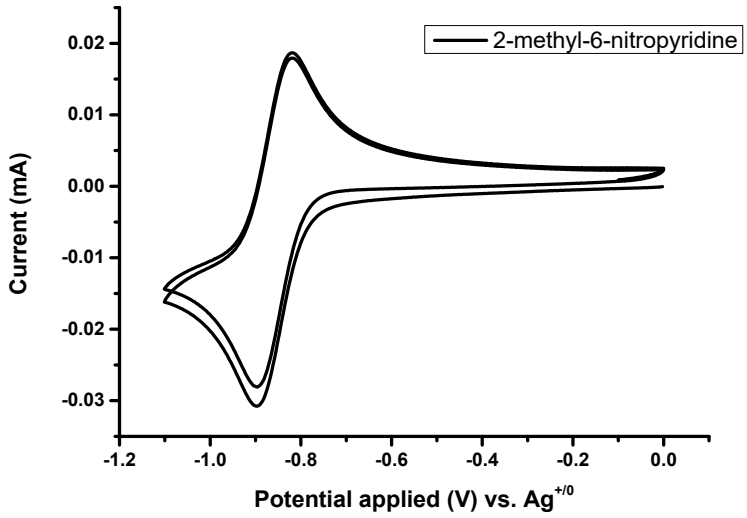

Figure S1. Cyclic voltammogram of 2-methyl-6-nitropyridine (**1**).

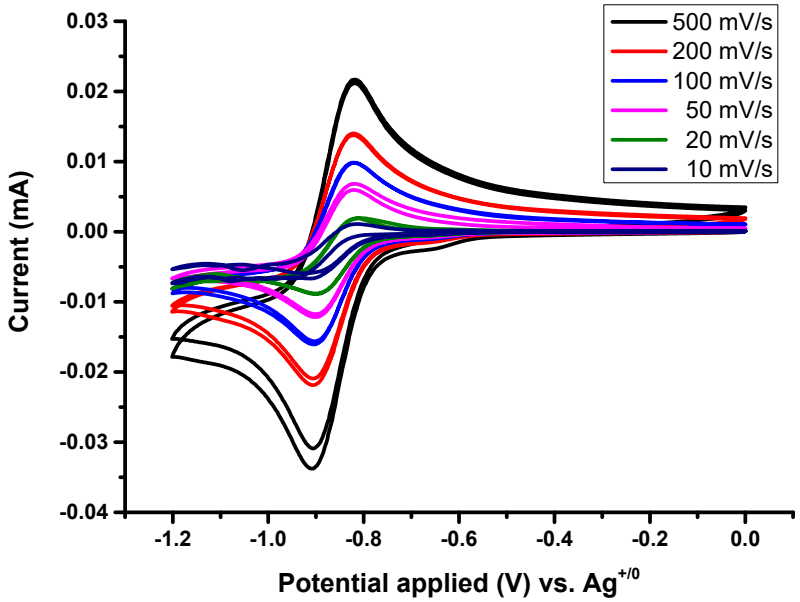

Figure S2. Cyclic voltammograms at different scan rates for $\mathbf{L_1}$.

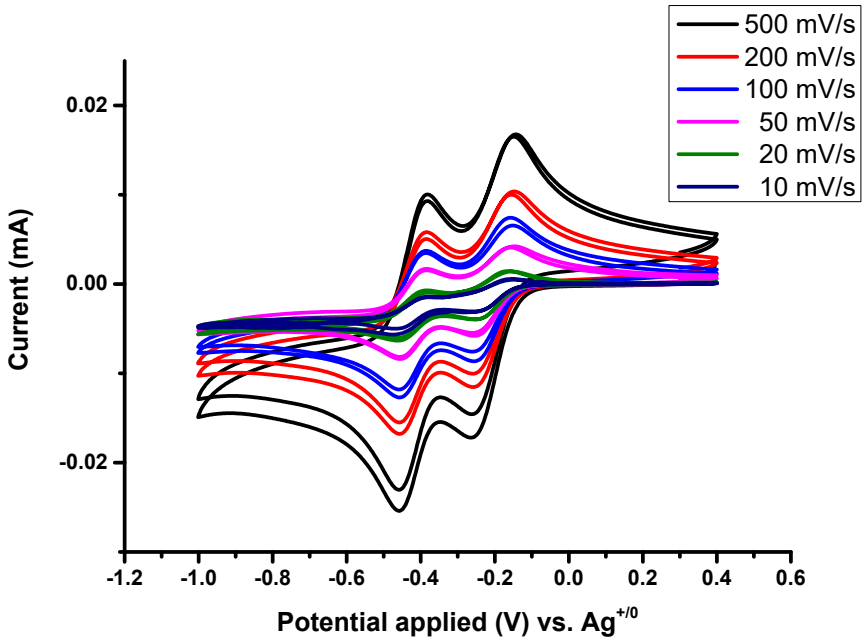

Figure S3. Cyclic voltammograms at different scan rates for $\mathbf{CaL_1^{2+}}$.

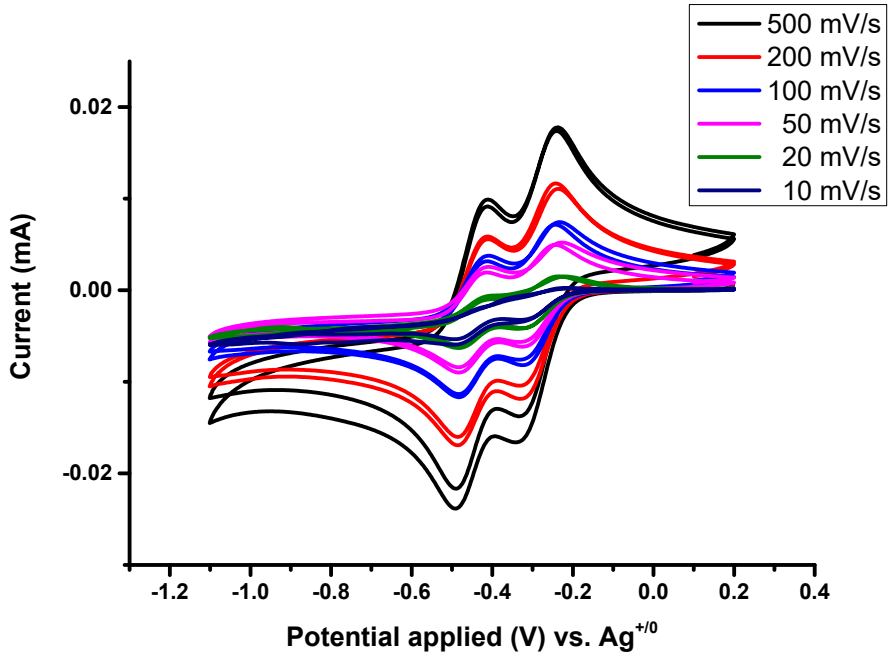

Figure S4. Cyclic voltammograms at different scan rates for $\mathbf{SrL_1}^{2+}$.

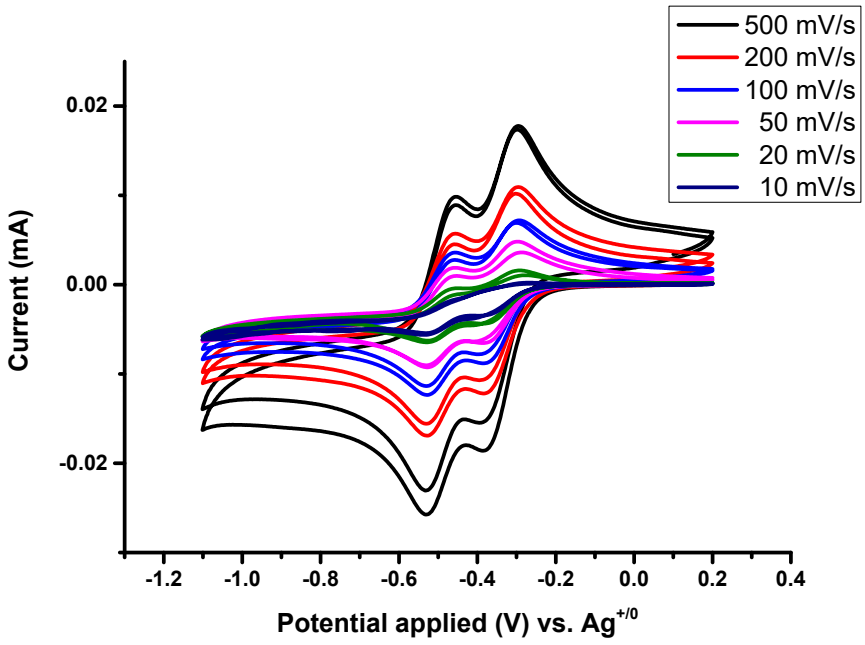

Figure S5. Cyclic voltammograms at different scan rates for $\mathbf{BaL_1}^{2+}$.

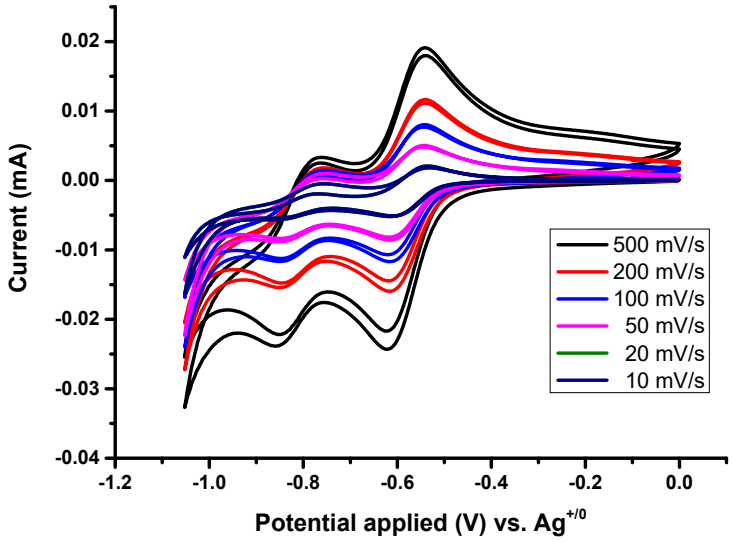

Figure S6. Cyclic voltammograms at different scan rates for $\mathbf{NaL_1^+}$.

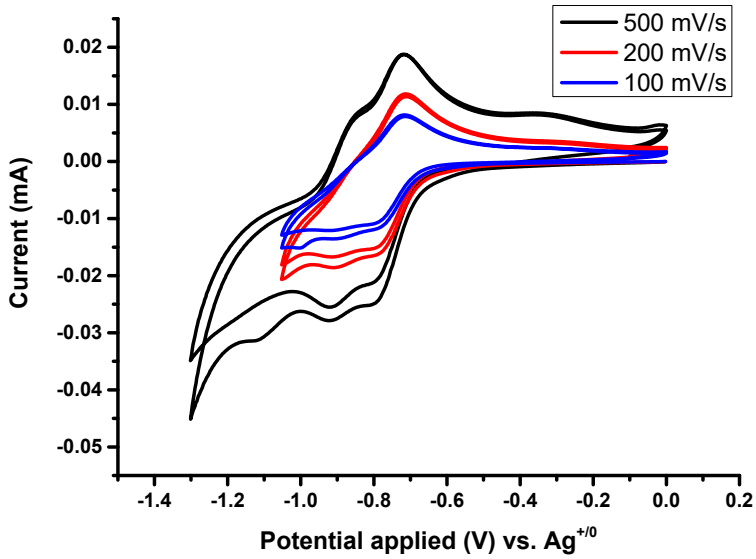

Figure S7. Cyclic voltammograms at different scan rates for $\mathbf{KL_1^+}$.

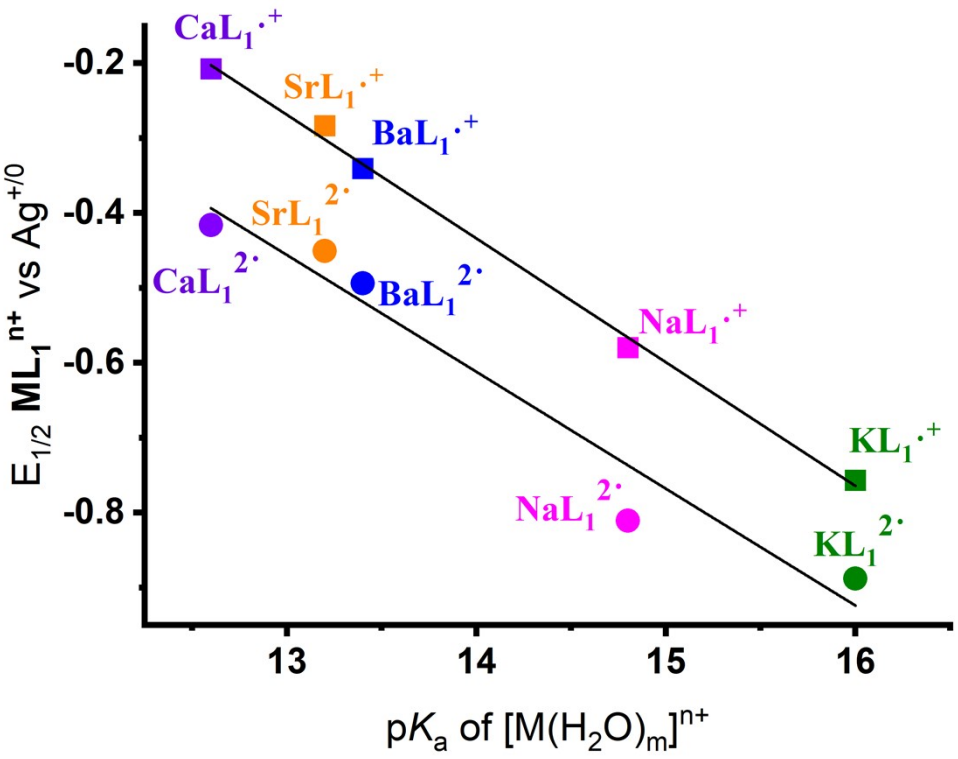

Figure S8. Correlation between the first and second half wave potentials observed in CV measurements and the pK_a of the aqua ion.

Analysis of electrochemical experiments.

Cyclic voltammograms exhibit a diffusion-controlled behavior, although the observed electron transfer reactions are not ideally reversible (so- called quasi-reversible). This leads to a peak separation between anodic and cathodic processes higher than 59 mV.[2]

The number of electrons involved in the reaction has been estimated using Randles-Sevcik Equation (Equation S1). Using this equation, and for values $D=1\cdot10^{-5}$ cm^2/s,[3] v=0.1 V/s, $C=1\cdot10^{-6}$ mol/cm^3 and A=0.0314 cm^2, a theoretical peak current of 23.9 μA for a 2-electron process, and 8.5 μA for a 1-electron process is obtained. The value obtained for the reduction of $\mathbf{L_1}$ is 17 μA. Considering the non-reversibility of the system, which leads to lower experimental currents than those predicted by equation S1,[4] . In our case, the experimental current is expected to be lower than reversible current by a factor of 0.8 (Matsuda parameter K.[4] With these data, an electron number of 1.86 e- for the standard equation, and 1.9 e- for the equation corrected by Matsuda parameters is obtained, confirming that a 1-electron process is impossible to be occurring, and a 2-electron process is taking place.

Equation S1. $$i_p = 0.4463nFAC\sqrt{\frac{FvD}{RT}}$$

Since, as stated above, the electrochemical reactions are quasi-reversible, heterogeneous rate constants (k^0), can be calculated using the Nicholson equation (Equation S2).[5]

Equation S2. $$k^0 = \sqrt{\left(\frac{\pi DnFv}{RT}\right)\psi}$$

Ψ is the Nicholson parameter, which is obtained empirically from nΔE_p using the Equation S3 when ΔE_p is lower than 200 mV:[6]

Equation S3. $$\psi = \frac{-0.6288 + 0.0021 \cdot n\,\Delta E_p}{1 - 0.0017 \cdot n \cdot \Delta E_p}$$

Where ΔE_p is the anodic-cathodic peak separation.

As can be seen in **Table S1**, a larger peak separation implies slower charge transfer rate. For bivalent cations, the peak separation for the first wave decreases with ionic radius, while the second wave exhibits an almost constant peak separation. This is attributed to the effect of cation charge density in the conformational changes and/or solvent reorganization energy needed for the charge transfer to occur.[7] First step involves the reduction of a highly charged complex, which will involve high reorganization energies, while the second step ends up in a neutral species, involving much less reorganization/solvation energy (see DFT calculations). For analogous alkaline cations, one would expect a faster first electron transfer and a slower second one, for the same reasons. This is particularly evident for sodium. In the case of potassium (lower charge density), deviations appear, indicating a possible change in charge transfer mechanism.

Table S1. Nicholson parameter and heterogeneous rate constants obtained for all the metallic complex of **L_1** studied in this work.

Sample	**$n\Delta E_p$/mV**	**$\Psi_{Nicholson}$**	**k^0/cm·s^{-1}**
Calcium 1st wave	116	0.3962963	0.008203223
Calcium 2nd wave	77	1.5116505	0.031290742
Strontium 1st wave	112	0.4353982	0.009012622
Strontium 2nd wave	78	1.4263804	0.029525675
Barium 1st wave	90	0.8298113	0.017176862
Barium 2nd wave	75	1.7138182	0.035475557
L_1	153	0.192067458	0.003680822
Sodium 1st wave	85	1.0119101	0.020946256
Sodium 2nd wave	95	0.6980488	0.014449415
Potassium 1st wave	100	0.5982857	0.012384347
Potassium 2nd wave	83	1.1058394	0.022890567

4. Determination of the affinity constant of L_1 for Ca^{+2}

UV/vis spectra were recorded with a ThermoScientifc Genesys 50 spectrophotometer with a quartz cell (path length: 1 cm). The formation of the $\mathbf{CaL_1}^{2+}$ complex was monitored by spectrophotometric titrations at 25ºC on a 10^{-5} M solution of the ligand $\mathbf{L_1}$ in CH_3CN. Typically, aliquots of a fresh standard solution of $Ca(TfO)_2$ ($TfO^- = CF_3SO_3^-$) in the same solvent were added and the UV/vis spectra of the samples were recorded. The latter solution contained a 10^{-5} M concentration of the ligand to avoid dilution during the course of the titration. The ionic strength was adjusted to using 0.1 M tetrabutylammonium hexaflorophosphate (TBAPF). The titration profiles evidenced the formation of four simultaneous isosbestic points at 224, 247, 260 and 278 nm during the course of the titration. This is indicative of the presence of a single equilibrium in solution, consistent with the formation of a 1:1 (Ca^{2+}:$\mathbf{L_1}$) complex. The analysis of the titration data provided the stability constant of the resulting complex by using a simultaneous fit of the UV/vis spectral changes in the range of 215-350 nm with the HYPERQUAD program.[8]

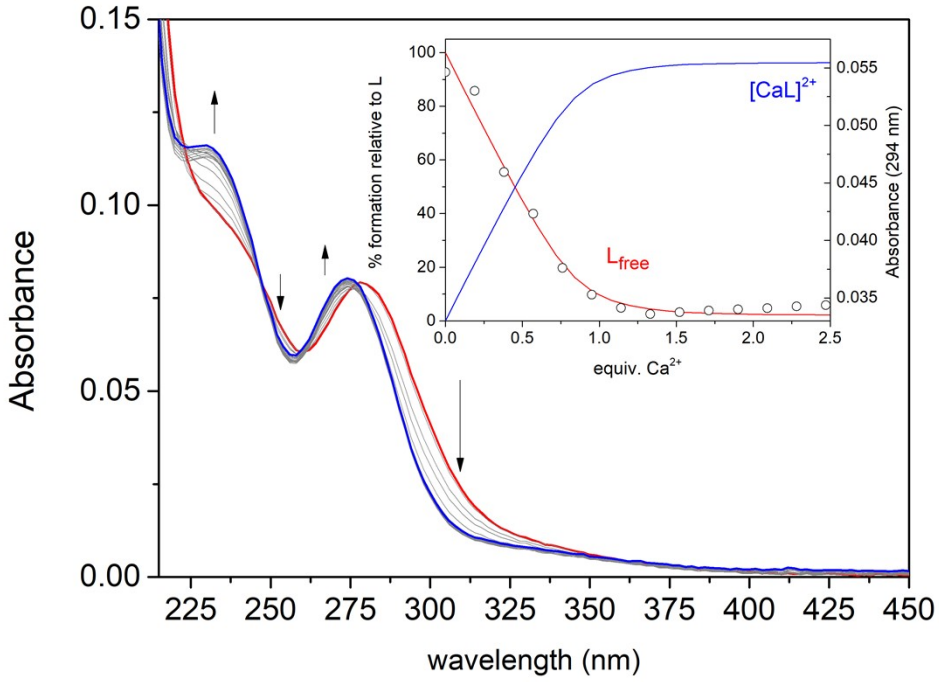

Figure S9. Family of UV/vis spectra taken during the course of the titration of ligand L_1 (10^{-5} M in CH_3CN) with a standard solution of $Ca(TfO)_2$ (1.2×10^{-3} M prepared in a 10^{-5} M solution of the same ligand in CH_3CN). Insert: titration profile at a selected wavelength vs. Ca^{2+}equivalents and species distribution diagram.

The stabilities of the $\mathbf{CaL_1}^{\bullet+}$ and $\mathbf{CaL_1}^{2\bullet}$ complexes were estimated from the CV data.[9] The equilibrium constants of the Ca^{2+} complexes are defined as in Equations S4 and S5:

$$Ca^{2+} + L_1 \rightarrow CaL_1^{2+} \qquad K_{CaL} = \frac{[CaL_1^{2+}]}{[Ca][L_1]}$$

Equation S4.

$$Ca^{2+} + L_1^{\cdot -} \rightarrow CaL_1^{\cdot +} \qquad K_{CaL^{\cdot -}} = \frac{[CaL_1^{\cdot +}]}{[Ca][L_1^{\cdot -}]}$$

Equation S5.

The reduction potential of the free ligand was estimated from the half wave potentials $E_{1/2}$ observed in the CVs. The reduction potentials of the ligand and the complex are then expressed as:

$$L_1 + e^- \rightarrow L_1^{\cdot -} \qquad E_L = \frac{-RT}{F} \ln \frac{[L_1^{\cdot -}]}{[L_1]}$$

Equation S6.

$$CaL_1^{2+} + e^- \rightarrow CaL_1^{\cdot +} \qquad E_{CaL} = \frac{-RT}{F} \ln \frac{[CaL_1^{\cdot +}]}{[CaL_1^{2+}]}$$

Equation S7.

Thus, the difference in reduction potential of the ligand and the metal complex can be related to the equilibrium constants for the formation of the complexes:

$$E_{CaL} - E_L = \frac{RT}{F} \ln \frac{[CaL_1^{\cdot +}][L_1]}{[CaL_1^{2+}][L_1^{\cdot -}]}$$

Equation S8.

$$E_{CaL} - E_L = \frac{RT}{F} \ln \frac{K_{CaL^{\cdot -}}}{K_{CaL}}$$

Equation S9.

Since the value of K_{CaL} was obtained independently from spectrophotometric experiments, the stability constant of the reduced complex can be obtained using Equation S9. Analogous expressions allow determining the association constant of the complex with the doubly reduced ligand $\mathbf{CaL_1^{2\bullet}}$.

5. DFT calculations

All density functional theory (DFT) calculations were performed with the Gaussian 16 program package[10] and the wB97XD functional,[11,12] which includes empirical dispersion. The triple-ζ quality Def2-TZVP[13] basis set was used throughout. Geometry optimizations were followed by analytical frequency calculations, which confirmed that the optimized geometries correspond to local energy minima. An ultrafine integration grid was used. A careful exploration of the conformational space was carried out following previous studies on crown-ether derivatives.[14,15] These calculations showed that the Δ(δλδ)(δλδ) conformation is the most stable one for the three complexes ($\mathbf{CaL_1^{2+}}$, $\mathbf{CaL_1^{\bullet +}}$ and $\mathbf{CaL_1^{2\bullet}}$), as observed for the large lanthanide(III) ions and Ac(III).[15,16] Single-point energy calculations were carried out using the SMD solvation model[17] to determine solvation free energies in acetonitrile. The free energies for the two reduction processes in acetonitrile solution, $\Delta G^{o}_{I\,(sol)}$ and $\Delta G^{o}_{II\,(sol)}$ were estimated using the thermodynamic cycle shown in Scheme S2.

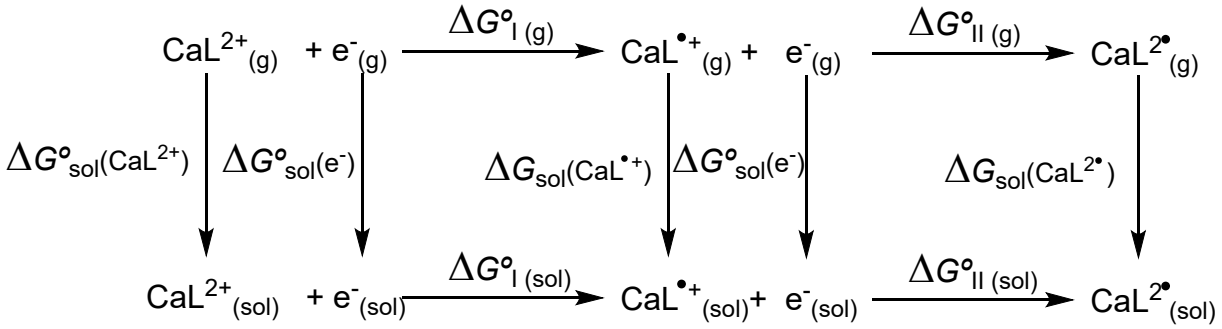

Scheme S2. Thermodynamic cycle used to calculate the free energies of the reduction processes.

Thus, $\Delta G^{o}_{I\,(sol)} = \Delta G^{o}_{I\,(g)} + \Delta G^{o}_{sol\,(CaL^{\bullet+})} - \Delta G^{o}_{sol\,(CaL^{2+})} - \Delta G^{o}_{sol\,(e^-)}$, and $\Delta G^{o}_{II\,(sol)} = \Delta G^{o}_{II\,(g)} + \Delta G^{o}_{sol\,(CaL^{2\bullet})} - \Delta G^{o}_{sol\,(CaL^{\bullet+})} - \Delta G^{o}_{sol\,(e^-)}$. The value of $\Delta G^{o}_{sol\,(e^-)}$ in acetonitrile solution was estimated to be -90.9 kJ mol^{-1} using the methodology reported previously.[18] The free energy of the electron in the gas phase was taken as -3.6160 kJ mol^{-1}. The different thermodynamic parameters are listed in Table S2.

Table S2. Values of Gibbs free energies (kJ mol^{-1}) obtained with DFT calculations.

$\Delta G^{o}_{I\,(g)}$	-744.6	$\Delta G^{o}_{II\,(g)}$	-460.6
$\Delta G^{o}_{sol\,(CaL^{\bullet+})}$	-234.9	$\Delta G^{o}_{sol\,(CaL^{2\bullet})}$	-124.6
$\Delta G^{o}_{sol\,(CaL^{2+})}$	-603.1	$\Delta G^{o}_{II\,(sol)}$	-259.4
$\Delta G^{o}_{I\,(sol)}$	-285.7		

The interaction energies between the aromatic units in $\mathbf{CaL_I^{2+}}$, $\mathbf{CaL_I^{\bullet+}}$ and $\mathbf{CaL_I^{2\bullet}}$ were estimated by taking the geometries of the two pendant arms from the optimized structures. The crown moiety of the receptor and the metal ion where removed and H the positions of the arms (2-nitropyridine, 2-NP) were optimized. Subsequently, the interaction energy was estimated as:

$$E(\text{2-NP})_{dimer} - 2\times E(\text{2-NP})_{dimer}$$

The results provide a strong repulsive interaction among the radical anion of the two 2-NP units of 237 kJ mol^{-1}.

REFERENCES

1 V. V. Pavlishchuk and A. W. Addison, Conversion constants for redox potentials measured versus different reference electrodes in acetonitrile solutions at 25°C, *Inorg. Chim. Acta*, 2000, **298**, 97–102.

2 A. J. Bard and L. R. Faulkner, *Electrochemical Methods: Fundamentals and Applications*, Wiley, New York, 2nd edn., 2000.

3 E. Yumet, H. Chen and S. Chen, Tracer diffusion of carbon tetrachloride, S-trioxane, 12-crown-4, 15-crown-5, 18-crown-6 in acetonitrile, benzene, and chlorobenzene, *AIChE Journal*, 1985, **31**, 76–81.

4 H. Matsuda and Y. Ayabe, Zur Theorie der Randles-Sevčikschen Kathodenstrahl-Polarographie, *Z. Elektrochem.*, 1955, **59**, 494–503.
5 R. S. Nicholson and Irving. Shain, Theory of Stationary Electrode Polarography. Single Scan and Cyclic Methods Applied to Reversible, Irreversible, and Kinetic Systems., *Anal. Chem.*, 1964, **36**, 706–723.
6 E. P. Randviir, A cross examination of electron transfer rate constants for carbon screen-printed electrodes using Electrochemical Impedance Spectroscopy and cyclic voltammetry, *Electrochim. Acta*, 2018, **286**, 179–186.
7 B. Fabre, J.-P. Desvergne, M. Colomès and J. Simonet, Electrochemical oxidation in different media of bis(p-phenylene crown ether) as a symmetrical molecule bearing two identical redox centers, *J. Electroanal. Chem.*, 1999, **460**, 119–134.
8 P. Gans, A. Sabatini and A. Vacca, Investigation of equilibria in solution. Determination of equilibrium constants with the HYPERQUAD suite of programs, *Talanta*, 1996, **43**, 1739–1753.
9 M. Regueiro-Figueroa, J. L. Barriada, A. Pallier, D. Esteban-Gómez, A. de Blas, T. Rodríguez-Blas, É. Tóth and C. Platas-Iglesias, Stabilizing Divalent Europium in Aqueous Solution Using Size-Discrimination and Electrostatic Effects, *Inorg. Chem.*, 2015, **54**, 4940–4952.
10 M. J. Frisch, G. W. Trucks, H. B. Schlegel, G. E. Scuseria, M. A. Robb, J. R. Cheeseman, G. Scalmani, V. Barone, G. A. Petersson, H. Nakatsuji, X. Li, M. Caricato, A. V. Marenich, J. Bloino, B. G. Janesko, R. Gomperts, B. Mennucci, H. P. Hratchian, J. V. Ortiz, A. F. Izmaylov, J. L. Sonnenberg, Williams, F. Ding, F. Lipparini, F. Egidi, J. Goings, B. Peng, A. Petrone, T. Henderson, D. Ranasinghe, V. G. Zakrzewski, J. Gao, N. Rega, G. Zheng, W. Liang, M. Hada, M. Ehara, K. Toyota, R. Fukuda, J. Hasegawa, M. Ishida, T. Nakajima, Y. Honda, O. Kitao, H. Nakai, T. Vreven, K. Throssell, J. A. Montgomery Jr., J. E. Peralta, F. Ogliaro, M. J. Bearpark, J. J. Heyd, E. N. Brothers, K. N. Kudin, V. N. Staroverov, T. A. Keith, R. Kobayashi, J. Normand, K. Raghavachari, A. P. Rendell, J. C. Burant, S. S. Iyengar, J. Tomasi, M. Cossi, J. M. Millam, M. Klene, C. Adamo, R. Cammi, J. W. Ochterski, R. L. Martin, K. Morokuma, O. Farkas, J. B. Foresman and D. J. Fox, *Gaussian 16 Rev. C.01*, Wallingford, CT, 2016.
11 J.-D. Chai and M. Head-Gordon, Long-range corrected hybrid density functionals with damped atom–atom dispersion corrections, *Phys. Chem. Chem. Phys.*, 2008, **10**, 6615–6620.
12 J.-D. Chai and M. Head-Gordon, Systematic optimization of long-range corrected hybrid density functionals, *J. Chem. Phys.*, 2008, **128**, 084106.
13 F. Weigend and R. Ahlrichs, Balanced basis sets of split valence, triple zeta valence and quadruple zeta valence quality for H to Rn: Design and assessment of accuracy, *Phys. Chem. Chem. Phys.*, 2005, **7**, 3297–3305.
14 A. Roca-Sabio, M. Mato-Iglesias, D. Esteban-Gómez, É. Tóth, A. de Blas, C. Platas-Iglesias and T. Rodríguez-Blas, Macrocyclic Receptor Exhibiting Unprecedented Selectivity for Light Lanthanides, *J. Am. Chem. Soc.*, 2009, **131**, 3331–3341.
15 A. Kovács, Theoretical Study of Actinide Complexes with Macropa, *ACS Omega*, 2020, **5**, 26431–26440.
16 M. Regueiro-Figueroa, D. Esteban-Gómez, A. de Blas, T. Rodríguez-Blas and C. Platas-Iglesias, Understanding Stability Trends along the Lanthanide Series, *Chem. Eur. J.*, 2014, **20**, 3974–3981.
17 A. V. Marenich, C. J. Cramer and D. G. Truhlar, Universal Solvation Model Based on Solute Electron Density and on a Continuum Model of the Solvent Defined by the Bulk Dielectric Constant and Atomic Surface Tensions, *J. Phys. Chem. B*, 2009, **113**, 6378–6396.
18 Z. Marković, J. Tošović, D. Milenković and S. Marković, Revisiting the solvation enthalpies and free energies of the proton and electron in various solvents, *Comput. Theor. Chem.*, 2016, **1077**, 11–17.